I&EC research
Industrial & Engineering Chemistry Research
pubs.acs.org/IECR
Article

Use, Preparation, and Characterization of Copper-Containing Silica Gel

Sevgi Ulutan, A. Pinar Tüzüm Demir, and Devrim Balköse*

Cite This: *Ind. Eng. Chem. Res.* 2020, 59, 9939−9949
Read Online

ABSTRACT: The preparation and characterization of humidity-indicating silica gel containing copper sulfate were aimed at in the present study. The equilibrium and kinetics of Cu(II) sorption were investigated by contacting 200−1600 mg dm^{-3} Cu ion-containing solutions with silica hydrogel slabs having 10% silica. The diffusion coefficient of Cu(II) in silica hydrogel was determined to be on the order of 10^{-10} m^2 s^{-1}. X-ray diffraction indicated that the gels contained mainly $CuSO_4 \cdot 3H_2O$, $CuSO_4 \cdot H_2O$, and small amounts of $CuSO_4$ and $CuSiO_3 \cdot 2H_2O$. The silica gel with Cu(II) can be used as a humidity indicator since its color changes from light blue to dark blue upon moisture adsorption.

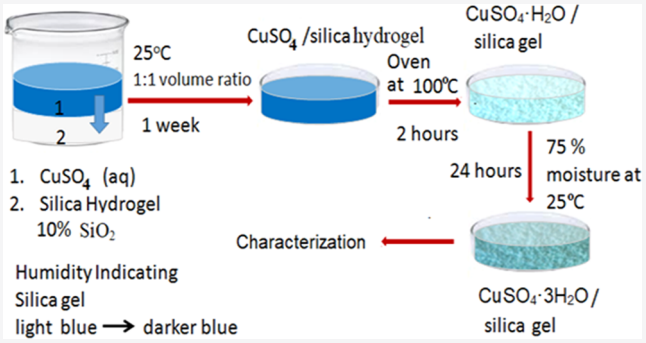

1. INTRODUCTION

Copper(II)-containing silica gels could be used as humidity indicators. Humidity-indicating silica gels change their color when their moisture content reaches a certain value. Silica gel with Co(II) is blue when dry and turns pink upon moisture absorption.[1] Co(II) compounds are expensive, and it would be more economical to use cheaper Cu(II) compounds for the same purpose. Humidity-indicating gels, light blue in dry form and dark blue in moist form, were obtained by dispersing copper sulfate in silica gel.[2] Silica gel could be prepared as xerogels by conventional drying, while as aerogels by supercritical extraction or freeze-drying. The mass transfer rate in column drying could be improved using silica gels as column fillings. These fillings can be produced in various shapes, such as porous monoliths with straight channels (microhoneycombs), fibers with polygonal cross sections, and powders, by means of unidirectional freezing of silica hydrogels.[3]

Cu(II) ions could be adsorbed by silica. Cu(II) adsorption by mesoporous silica of different pore sizes in the range 4−8 nm indicated that the mobility of Cu(II) ions increases as the pore size decreases, leading to an increase in adsorption rates. This was attributed to the change in properties of water when confined in a nanoporous environments. When a fluid resides in a nanoporous environment, the observed density, surface tension, and dielectric constant diverge from those measured in the bulk. Knight et al.[4] attributed these effects to the deviations in fundamental water properties as the pore diameter decreases. In particular, these effects were most notable in SBA-15 (silica with 4 nm pore size), where the changes in water properties may be responsible for the enhanced Cu mobility and, therefore, faster Cu adsorption kinetics. Batch adsorption isotherms were fitted to adsorption models (Langmuir, Freundlich, and Dubinin−Radushkevich), and adsorption kinetic data were fitted to a pseudo-first-order reaction model.[4]

Ren et al.[5] prepared a Cu(II) ion-imprinted polymer using Cu(II) ions as a template, *N*-[3-(2-aminoethylamino)propyl]-trimethoxysilane (AAPTMS) as a functional monomer, and tetraethyl orthosilicate (TEOS) as a cross-linker. They found that the adsorption by the ion-imprinted polymer was so fast that the adsorption equilibrium was reached within 60 min. The adsorption capacity of the Cu(II) ion-imprinted polymer (with a maximum of almost 40 mg g^{-1}) was always larger than that of the nonimprinted one. The Cu(II) ion-imprinted polymer, which could be as well reused several times without significant loss of adsorption capacity, showed high selectivity and relative selectivity coefficients for Pb(II), Ni(II), Cd(II), and Co(II).[5]

Functionalized silicas were also prepared by Xue and Li[6] and Chiron et al.[7] Xue and Li[6] synthesized functionalized SBA-16 (porous silica with 5 nm pore size) mesoporous silica with −SH groups and employed it as an adsorbent for Cu(II) from aqueous solutions. They reported that the synthesized material possessed high-order adsorption capacity for Cu(II) ions and

Received: December 19, 2019
Revised: April 2, 2020
Accepted: April 30, 2020
Published: April 30, 2020

https://dx.doi.org/10.1021/acs.iecr.9b06950
Ind. Eng. Chem. Res. 2020, 59, 9939−9949

the maximum Cu(II) adsorption on this adsorbent occurred in the pH range of 5−6 with an adsorption capacity of 36.38 mg g^{-1}. The adsorption of Cu(II) on functionalized SBA-16 mesoporous silica fitted well to the Langmuir equation (R^2 = 0.9847).

Chiron et al.[7] studied the kinetics of the adsorption of copper(II) onto commercial silica that is grafted with an ethylenediamine derivative, *N*-[3-(trimethoxysilyl)propyl]-ethylene diamine, at 20 °C. They reported that the Langmuir model well described the adsorption of Cu(II). From the Langmuir isotherms, they calculated the maximum adsorption capacity of Cu(II) on the grafted silica as 0.261 mmol Cu(II) g^{-1} and that of nonmodified silica as 0.036 mmol Cu(II) g^{-1}. They reported that the best fit was obtained with the double-exponential model.

Composite materials from silica gel and chitosan were good adsorbents for copper ions, as well. Gandhi and Meenakshi[8] prepared a silica gel/chitosan composite by a sol−gel method and characterized it. They investigated the sorption of copper ions onto this composite. They reported that this composite has excellent metal sorption capacity than those of silica gel and chitosan. They reported that the equilibrium data complied well with the Freundlich isotherm model.

Copper silicate could be synthesized by many different methods using different starting materials. Anderson and Hochgesang[9] reported that 0.1 mol dm^{-3} copper sulfate and sodium silicate solutions mixed at the boiling point yielded basic copper sulfate and silica rather than copper silicate. The X-ray diffraction (XRD) pattern of hollow chemical garden fibers from sodium silicate and $CuSO_4$ showed that they contained $CuSO_4$ (peak at 2θ = 22.8°), $CuSiO_3{\cdot}3H_2O$ (0.26 nm (peak at 2θ = 33.5°)), and $Na_2Cu(SO_4)_2$ (peaks at 24.7, 33.4, and 35.7°).[10] Chemical garden tubes that were formed by injecting $CuSO_4$ solution from the bottom of the sodium silicate solution had smooth outer surface and spherical particles on the inner surface with diameters increasing with the flow rate of the injected solution.[11]

Chrysocolla, cryptocrystalline copper silicate with a proposed formula $(Cu_2H_2Si_2O_5)(OH)_4{\cdot}nH_2O$, is a secondary mineral occurring in the oxidized zones of copper deposits. Gel powders with Cu/Si ratios of 0.32, 0.83, and 1.61 were prepared from the solutions of $Cu(NO_3)_2$ and $Si(OC_2H_5)_4$ with Cu/Si molar ratios of 0.5, 1.0, and 2.0 respectively. The gels had chrysocolla-like middle-range ordering despite the variation in the Cu/Si molar ratios of the starting stock solutions.[12]

A facile route for fabricating copper silicate hierarchical double-walled hollow nanofibers by combining the electrospinning technique with the hydrothermal method was demonstrated by Jin et al.[13] Hollow spherical copper silicate spheres were obtained by reacting ammoniacal copper nitrate solution with colloidal silica at 140 °C in an autoclave. Basic ammoniacal solution dissolved silica from the surface of the particles to form a copper silicate layer. Silica particles coated with silica further reacted with OH^- ions; thus, a copper silicate crust with increasing thickness was formed. The XRD pattern of the product showed that it was copper silicate (JCPDS 03-0219).[14] Hierarchically hollow structured copper silicate materials were synthesized directly from the core−shell-structured templates based on confined chemical reactions between the solid matter of a core and shell under hydrothermal conditions.[15] By a novel method, core−shell-structured Cu_2O@mSiO_2 (m = mesoporous) was transformed to tubular copper silicate assemblages (TCSAs). Depending on the original shapes of Cu_2O, TCSA could be tailored as spherical or cubic assemblages with stacking copper silicate nanotubes (inner diameter, 4.5 nm; thickness, 0.8 nm; length, ca. 96 nm) in the shell. Mesoporous $Na_4[Cu_2Si_{12}O_{27}(OH)_2]$-$[(NaOH)_2(H_2O)_6]$ (CuSH−1Na) was synthesized by a simple hydrothermal method in an autoclave at 230 °C.[16] Ion exchange of Na^+ by Cs^+, Ca^{2+}, and Sr^{2+} ions showed that the structure can suffer partial replacement of the charge-compensating cations. Nanoporous copper silicates with one-dimensional 12-ring channel systems, $Na_4[Cu_2Si_{12}O_{27}[OH]_2[(AOH)(NaOH)](H_2O)_6]$, (CuSH−1A) where A = Na, K, Rb, and Cs, were synthesized by dissolving fumed silica in NaOH and AOH mixture and by adding copper sulfate to this solution. The final solutions were heated at 230 °C in an autoclave.[17] Microporous $Na_2CuSi_5O_{12}$ (SG29) was synthesized and used for CO_2 capture from humid flue gases and the humid atmosphere. SG29 had H_2O-specific and CO_2-specific adsorption sites but did not have H_2O/CO_2-sharing sites. Therefore, it readily adsorbs both H_2O and CO_2 from the humid flue gases and the atmosphere, but the adsorbing H_2O does not interfere with the adsorption of CO_2. It is also highly stable after the adsorption of H_2O and CO_2 because it is synthesized hydrothermally.[18]

Copper-containing silica aerogels were prepared from tetramethyl orthosilane (TMOS), methanol, ammonia, ethanol, and $Cu(NO_3)_2{\cdot}3H_2O$.[19] Aerogels with 0.11 cm^3 g^{-1} density were obtained with supercritical ethanol extraction at 250 °C.[19]

Silica-supported copper catalysts derived from copper phyllosilicates were synthesized by Jiang et al.[20] Ammonia aqueous solution and $Cu(NO_3)_2{\cdot}3H_2O$ were mixed in deionized water under vigorous stirring. Colloid silica (LUDOX HS30, Sigma-Aldrich) was then added into the mixture with a controlled pH value in the range of 11−12 and stirred for 24 h. The obtained suspension was heated in a water bath at 80 °C to allow ammonia evaporation gradually. The obtained mixture was transferred into a hydrothermal bomb and treated at 150 °C for 24 h. The precipitates were filtered, washed with deionized water, dried at 120 °C for 4 h, and calcined at 400 °C in air. Copper phyllosilicates were obtained by this method. In the XRD pattern, weak signals at 30.8, 35.0, 57.5, and 62.4°, corresponding to the diffraction pattern of $Cu_2Si_2O_5(OH)_2$, were identified.[20]

Magnetic hierarchical copper silicate hollow nanotubes and magnetic carbon nanotubes with a hierarchical copper silicate nanostructure for the efficient adsorption and removal of hemoglobin were synthesized by Zhang et al.[21,22] All weak diffraction peaks of the X-ray diffraction (XRD) pattern were clearly indexed to copper silicate (JCPDS card no. 32-0346). The apparent broadening and overlapping of all of these peaks indicated that the as-prepared copper silicates were composed of nanoscale crystals.[22]

In the present study, the preparation and characterization of humidity-indicating silica gel by treating silica hydrogel with a copper sulfate solution were aimed at. The equilibrium and kinetics of copper(II) ions sorption in silica hydrogel were investigated by atomic absorption spectroscopy and the indicating silica gels were characterized by differential scanning calorimetry (DSC), infrared (IR) spectroscopy, XRD, visible spectroscopy, and moisture adsorption from air with controlled humidity for this purpose.

https://dx.doi.org/10.1021/acs.iecr.9b06950
Ind. Eng. Chem. Res. 2020, 59, 9939−9949

2. MATERIALS AND METHODS

Silica Hydrogel Preparation. Silica hydrogel was prepared by simplifying the previously used method.[23] First, sodium silicate solution (Sigma-Aldrich, d = 1.390 g mL^{-1} with 14% (w/w) NaOH and 27% (w/w) SiO_2) was diluted with an equal volume of deionized water. Then, while being stirred with a mechanical stirrer (Thermal Kundel), a diluted sodium silicate solution was added by a diaphragm pump (Cole-Palmer) at a slow rate into 1.5 mol dm^{-3} H_2SO_4 (Merck, 98%) solution until the pH was equal to 1.0 to prepare the silica hydrosol. The pH was monitored using a pH meter (EMAF EM78X). Aliquots of 50 cm^3 of the silica sol were allowed to gel in glass jars for one day at 25 °C. Silica hydrogel obtained in each jar was washed with an equal volume of water 10 times for 30 min to remove byproduct sodium sulfate and excess acid. The layer thickness of the silica hydrogels in jars was 7 mm, and the pH of the final wash solution was 2.0.

Cu(II) Sorption Experiments. The effects of Cu(II) concentration on its adsorption kinetics were investigated by adding Cu(II) solutions prepared from $Cu(SO_4)_2{\cdot}5H_2O$ (Merck) onto silica hydrogel. The pH of the Cu(II) solution was regulated to 2 with H_2SO_4. Aliquots of 2 cm^3 were drawn from the solution phase at different time intervals, and their concentrations were determined by a Varian 10 BQ atomic absorption spectrophotometer at 224.6 nm.[24]

Indicating Silica Gel Preparation and Characterization. The silica hydrogel sample casts in glass jars were contacted with a saturated $CuSO_4{\cdot}5H_2O$ solution having 32.7 g of $CuSO_4{\cdot}5H_2O$ per 100 cm^3 water at 25 °C with 1:1 volume ratio for 1 week. The silica hydrogel phase was dried at 100 °C for 2 h after decanting the solution phase. $CuSO_4{\cdot}5H_2O$ and control silica gel without any copper ion were also dried for 2 h at 100 °C. The water vapor adsorption isotherm of the dried samples was determined by keeping the samples in air at different relative humidity values at 25 °C for 24 h. The relative humidity of the air was controlled by equilibration of air with the saturated salt solutions in glass desiccators. The DSC curves of $CuSO_4{\cdot}5H_2O$, pristine silica gel, and silica gel with copper sulfate that were in equilibrium with 75% relative humidity air at 25 °C were obtained using a Setaram DSC 92 at temperatures ranging from room temperature to 300 °C with 10 °C min^{-1} rate under 40 cm^3 min^{-1} N_2 gas flow.

The IR spectra of samples were obtained by a KBr disk method using a Shimadzu IR 470 infrared spectrometer. The XRD patterns of the samples were obtained using a JEOL X-ray diffractometer using Cu K_α radiation. The photographs of silica gel and dried and moisture-adsorbed copper sulfate samples were taken using a Redmi Note 8 Pro Al Quad camera. The drift visible spectrum of the dried and moisture-adsorbed sample pellets, pressed from the powders by a hydraulic press, were obtained using a Data color spectrophotometer.[25] The dried samples were stored in desiccators with $CaCl_2$ adsorbent. They were quickly weighed in ambient air for DSC and IR analyses to avoid moisture adsorption.

RESULTS AND DISCUSSION

Equilibrium of Cu(II) Sorption to Silica Hydrogel. The amount of Cu(II) ions on silica hydrogel in equilibrium with Cu(II) solutions were calculated using the data obtained by atomic absorption spectroscopy. The adsorption isotherm of Cu(II) onto silica hydrogel is shown in Figure 1.

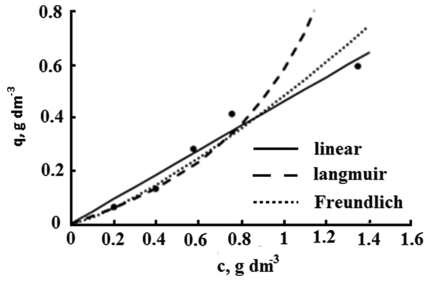

Figure 1. Adsorption isotherm of Cu(II) onto silica hydrogel and fits of experimental data to model equations.

The adsorption of Cu(II) from aqueous solution onto silica depends on the double layer potential. The farther the separation of the solution pH from the zero charge of the silica particles, the higher the adsorption of Cu(II) on the silica surface.[26] The isoelectric point of silica is reported as pH 1.7 or 2.02.[20,27] Since the difference in the solution pH at the equilibrium (around 2) and the isoelectric point of silica pH (1.7−2.0) is very small, the amount of Cu(II) adsorbed on the silica particles should be very small[26] and Cu(II) should remain in the aqueous phase of silica hydrogel. The adsorption data were fitted to linear (eq 1), Langmuir (eq 3), and Freundlich (eq 5) adsorption models with R^2 values of 0.95, 0.98, and 0.97, respectively. Equations 2, 4, and 6 are the model equations found for linear, Langmuir, and Freundlich isotherms, respectively. The adsorption isotherms from model equations and experimental data are shown in Figure 1.

Linear model

$$q = Kc \tag{1}$$

$$q = 0.46c \tag{2}$$

$$R^2 = 0.95$$

Langmuir model

$$\frac{1}{q} = \frac{1}{(q_m K_L)}\frac{1}{C} + \frac{1}{q_m} \tag{3}$$

$$\frac{1}{q} = \frac{3.82}{c} - 2.1 \tag{4}$$

$$R^2 = 0.98$$

Freundlich model

$$q = k'c^n \tag{5}$$

$$q = 0.48\ c^{1.3} \tag{6}$$

$$R^2 = 0.97$$

where q is the concentration of Cu(II) (in g dm^{-3}) on silica hydrogel, c is the concentration of Cu (in g dm^{-3}) in the aqueous phase, K is the linear equilibrium constant, K_L is the Langmuir constant, q_m is the monolayer capacity of Cu(II) (in g dm^{-3}) on silica hydrogel, k' is the Freundlich constant, and n is the Freundlich exponent.

Even if the highest R^2 value was obtained for the Langmuir model, the adsorption data did not fit the Langmuir model since the q_m value found was negative, which was not a possible situation. The higher R^2 value for the Freundlich model indicated that the data fitted to this model better than the linear model. The linear model also has an R^2 value

https://dx.doi.org/10.1021/acs.iecr.9b06950
Ind. Eng. Chem. Res. 2020, 59, 9939−9949

comparable to that of the Freundlich model. If there was negligible adsorption on silica surfaces, the Cu(II) concentration in both aqueous phases would be the same since the volumes of the solution and silica hydrogel phases were equal and 95% of the silica hydrogel volume was water.[29] Thus, the equilibrium constant in eq 2 should be close to 1. However, it is found as 0.46. This could be explained by the presence of inaccessible pores in silica hydrogel. Indeed, Blomqvist et al.[28] showed that, by three-dimensional electron tomography, only 30−40% of the pore volume of silica hydrogels was accessible.

Kinetics of Cu(II) Sorption onto Silica Hydrogel. The changes in mass (M) of Cu(II) adsorbed onto silica hydrogel from the aqueous phase for different initial concentrations are depicted in Figure 2. The simultaneous processes that occur

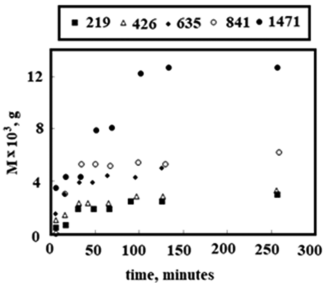

Figure 2. Amount of Cu(II) adsorbed onto silica hydrogel versus time for different initial concentrations (mg dm^{-3}) of Cu(II) in the solution.

during Cu(II) transport were thought to be the cause of the variations in solution concentrations. These simultaneous processes were water transport from the silica hydrogel phase to the aqueous phase and the transport of other ions such as H^+, Na^+, Cl^-, SO_4^{2-}, and SiO_4^{2-} between the phases. Thus, a simplified approach to describe quantitatively the transport of Cu(II) from the aqueous phase to the silica hydrogel phase would be useful.

The mass (M) adsorbed onto the silica hydrogel was found by integrating the concentration change of the solution versus time data. The silica hydrogel is a transparent substance. When Cu(II) ions diffuse in silica hydrogel, the diffused parts acquire the blue color of the copper solution. The color intensity is the measure of the concentration of Cu(II). Thus, evenly distributed blue color as observed herein throughout the silica hydrogel means the Cu(II) concentration is the same at every point. In other words, the Cu(II) distribution in silica hydrogel was homogeneous since the same blue color intensity was observed throughout the vertical cross section.

The sorption data of Cu(II) ions in silica hydrogel were fitted to different adsorption models such as the pseudo-first-order model (eq 7), pseudo-second-order model (eq 8), and solid diffusion model (eq 9).

Pseudo-first-order model

$$\ln\left[\frac{q_e - q}{q_e}\right] = -k_1 t \tag{7}$$

Pseudo-second-order model

$$\frac{t}{q} = \frac{1}{k_2 q_e^2} + \frac{1}{q_e} t \tag{8}$$

Solid diffusion model

$$\frac{M_t}{M_\infty} = \frac{4}{l}\sqrt{\frac{D_e t}{\pi}} \tag{9}$$

where k_1 is first-order rate constant, k_2 is the second-order rate constant, M_t and M_∞ are the amounts of Cu(II) ions transferred from the water phase to the silica hydrogel at any time and at equilibrium, respectively, and D_e is the effective diffusion coefficient.

The constants found by applying the experimental data in Figure 2 to different models and the R^2 values of the linear relations of the models in Figures 3−5 are shown in Table 1.

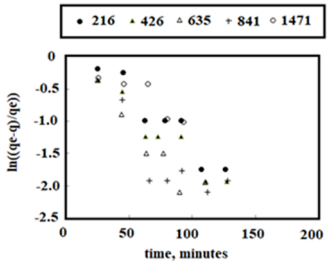

Figure 3. First-order reaction model for different initial concentrations (mg dm^{-3}) of Cu(II) in the solution.

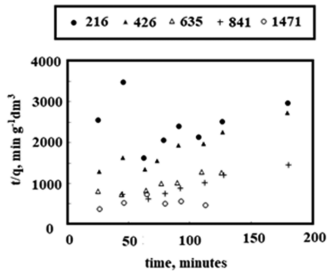

Figure 4. Second-order reaction model for different initial concentrations (mg dm^{-3}) of Cu(II) in the solution.

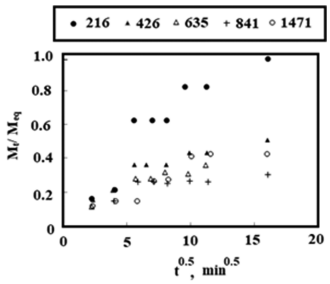

Figure 5. Solid diffusion model for different initial concentrations (mg dm^{-3}) of Cu(II) in the solution.

Since the data were of oscillating-type, low R^2 values were obtained for the applied models. The highest average R^2 value (0.83) was obtained for the first-order reaction model.

Even if the first-order reaction model had the highest correlation coefficient, the solid diffusion model was also considered as a plausible process. The effective diffusion coefficient of Cu(II) in silica hydrogel was calculated for the 5:1 solution-to-gel ratio using the slopes of M_t/M_∞ versus $t^{1/2}$ linear relations up to 60 min time period in Figure 5 using eq 9. The data were linear with a low correlation coefficient in the range of 0.58−0.92. The low correlation coefficient should be attributed to the oscillating nature of the process. The effective

https://dx.doi.org/10.1021/acs.iecr.9b06950
Ind. Eng. Chem. Res. 2020, 59, 9939−9949

Table 1. Kinetic Model Constants and Their R^2 Values

	first-order model		second-order model			solid diffusion model	
initial concentration (mg dm^{-3})	k_1 min^{-1}	R^2	q_e (mg dm^{-3})	k_2 (dm^3 mg^{-1} min^{-1})	R^2	$D_e \times 10^{10}$ (m^2 s^{-1})	R^2
219	0.013	0.86	0.89	0.001	0.01	2.8	0.80
426	0.016	0.92	0.11	0.089	0.92	0.9	0.41
635	0.02	0.89	0.18	0.056	0.86	0.7	0.58
841	0.019	0.71	0.16	0.120	0.92	0.3	0.44
1471	0.010	0.79	0.34	0.001	0.04	0.5	0.80
average	0.016	0.83	0.54	0.053	0.55	1.0	0.60

diffusion coefficients of Cu(II) for different initial Cu(II) concentrations are listed in Table 1. The effective diffusivities of various ions and substances in water and silica hydrogel are also reported in Table 2.[23,29−37] Substances such as malachite green and xylenol orange, that are strongly adsorbed onto silica gel, had very small diffusion coefficients in silica hydrogel since they diffuse in the adsorbed state. In the adsorbed state, breaking and reforming of physical bonds are needed. Therefore, diffusion becomes slower compared to the one in solution, where the substances can freely move toward lower concentrations. Also, the diffusion of ions in the hydrous silica gel was very small due to its lower porosity compared to that of silica hydrogel.[35] Since the preparation methods of silica gels in Table 2 are very different from each other, the silica/water ratio, porosity, and fraction of accessible pores are also different and this makes the correlation between diffusivity values not good enough. However, the average effective diffusion coefficient of Cu(II) in silica hydrogel of 1×10^{-10} m^2 s^{-1} is substantially lower than the diffusivity of Cu(II) in water,[33] 1.69×10^{-9} m^2 s^{-1}, indicating the existence of a tortoise path in silica hydrogel.

Table 2. Effective Diffusivities of Various Ions and Substances in Water, Silica Hydrogel, and Silica Gel

species	pH	medium	$D \times 10^9$ (m^2 s^{-1})	refs
protons	7	water	9. 1	23
protons	1−4	silica hydrogel	−17 + 21 pH −3.7 pH^2	23
protons	2	silica hydrogel	1.92 ± 0.56	29
NaCl	7	water	1.6	30, 31
$CoCl_2$	7	water	1.29−1.08	32
$CuCl_2$		water	1.69	33
$CoSO_4$	8−8.5	silica hydrogel	0.16	34
$CoCl_2$	8−8.5	silica hydrogel	0.27	34
$Co(NO_3)_2$	8−8.5	silica hydrogel	3.6	34
$CoCl_2$	6.8−10.8	hydrous silica gel	0.00686	35
Co(II)	2	silica hydrogel	13.5 ± 8.1	29
NaCl	7	silica hydrogel	1.57	30, 31
$Ni(NO)_3$		silica hydrogel	0.6	35
chromate	9	silica hydrogel from colloidal silica	0.176−0.848	36
malachite green	4.5−9	silica hydrogel from colloidal silica	0.14 ± 01	37
xylenol orange	4.5−9	silica hydrogel from colloidal silica	0.27 ± 0.2	37
Cu(II)	2	in silica hydrogel	10	present study

Characterization of Dried Silica Gels with and without Cu(II) Ions. *Drying and Moisture Adsorption of Silica Gel, Silica Gel with Copper Sulfate, and $CuSO_4 \cdot 5H_2O$.* Crystalline copper sulfate pentahydrate ($CuSO_4 \cdot 5H_2O$) contains two unique copper−water geometries.[38] Each copper cation is coordinated by four equatorial water molecules (two symmetrically unique water molecules on each), and are bridged by sulfate anions bonded at the axial positions, forming infinite polymeric chains. The fifth cocrystallized water molecule forms two hydrogen bonds with the bridging oxygen atoms of the adjacent chains and does not directly interact with the metal cations.[38] The phase diagram of the $CuSO_4$−water system indicated that the stable thermodynamic form of $CuSO_4$ hydrate in 75% relative humidity air at 25 °C is $CuSO_4 \cdot 3H_2O$.[39]

When $CuSO_4 \cdot 5H_2O$ is heated, first, $CuSO_4 \cdot 1/2H_2O$ forms, which is a mixture of $CuSO_4$, and then upon further heating $CuSO_4$ forms. $CuSO_4$ and $CuSO_4 \cdot H_2O$ are hygroscopic and transformed to $CuSO_4 \cdot 3H_2O$ upon moisture absorption. However, when amorphous $CuSO_4$ is rehydrated with liquid water, $CuSO_4 \cdot 5H_2O$ forms.[40] When $CuSO_4 \cdot 5H_2O$ is heated, dehydration occurs as per the following path, as indicated by eqs 10−14.[41]

$$CuSO_4 \cdot 5H_2O(c) \rightarrow CuSO_4 \cdot 3H_2O(c) + 2H_2O(l) \quad (10)$$

Localized pockets of saturated solution form from liberated water.

$$H_2O(l) + CuSO_4 \cdot xH_2O(c) \rightarrow (\text{saturated solution})(l) \quad (11)$$

$$(\text{saturated solution})(l) \rightarrow H_2O(g) + CuSO_4 \cdot 3H_2O(c) \quad (12)$$

$$CuSO_4 \cdot 3H_2O(c) \rightarrow CuSO_4 \cdot H_2O(c) + 2H_2O(g) \quad (13)$$

$$CuSO_4 \cdot H_2O(c) \rightarrow CuSO_4(c) + H_2O(g) \quad (14)$$

The thermogravimetric (TG) and DSC curves of $CuSO_4 \cdot 5H_2O$ were obtained at seven heating rates (b = 1, 3, 6, 10, 15, 20, and 30 K min^{-1}) by Cheng et al.[42] The DSC curves illustrate two major and remarkable endothermic peaks at the temperature ranges of 30−160 and 160−350 °C. From the differential heating rates, the TG curves exhibit three steps of mass loss. However, with an increase in heating rate, the demarcations between step I and step II become less and less obvious and their sum is called stage I. $CuSO_4 \cdot 5H_2O$ has lost four crystal water molecules in stage I, and the temperature range is 50−150 °C. One water molecule is lost in stage 3, and the temperature range is 173−260 °C.[42]

Copper sulfate pentahydrate dehydration was also studied using variable-temperature diffuse reflection infrared Fourier transform spectroscopy by White.[43] It was observed that in a static environment the dehydration proceeds sequentially from the pentahydrate to the trihydrate and then to the monohydrate. When helium purge was employed while heating

https://dx.doi.org/10.1021/acs.iecr.9b06950
Ind. Eng. Chem. Res. 2020, 59, 9939−9949

samples, the monohydrate was formed directly from the pentahydrate.

Infrared spectral features showed that in a static environment the lattice water molecules were involved in coordinated motions, which were absent when purge was employed.

The differences between crystal structures obtained in the static and purge environments were explained by the dependence of equilibrium processes on the local water vapor concentration and lattice water environment, respectively.[43]

The copper compounds in silica gel and their hydration levels were not known exactly. The material balance indicated that silica gel could have a maximum of 40.6% $CuSO_4$, assuming that it was present as anhydrous copper sulfate. Further analysis of the sample would give more information about its composition.

The DSC curves of copper sulfate pentahydrate, silica gel, and silica gel with copper sulfate are shown in Figure 6. The

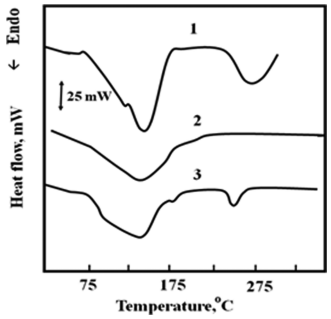

Figure 6. DSC curves of (1) copper sulfate pentahydrate, (2) silica gel, and (3) silica gel with copper sulfate in equilibrium with 75% relative humidity air at 25 °C.

DSC curve of copper sulfate pentahydrate herein also showed mainly two endothermic peaks with 151 and 275 °C maxima, close to the values (151 and 283 °C) reported by Cheng et al. There was a shoulder at 125 °C for the first peak as well. The first peak at 151 °C and the second peak at 275 °C belonged to the loss of four moles of water and one mole of water from $CuSO_4 \cdot 5H_2O$, respectively.[42] On the other hand, silica gel has only one broad endotherm belonging to the desorption and evaporation of adsorbed water, being maximum at 132 °C.

However, silica with copper sulfate had a different DSC curve than those of copper sulfate pentahydrate and silica gel. It had two main peaks at 151 and 247 °C and a small shoulder at 186 °C to the first peak.

Since the samples in the present study were heated for drying at 100 °C for 2 h, only partial dehydration of copper sulfate should have occurred. The silica gel sample with copper sulfate also contained, not pure copper sulfate, other products that could be formed by the reaction of silica hydrogel and copper sulfate.

Water Vapor Adsorption Isotherms. The water vapor adsorption isotherms of the samples are shown in Figure 7. Silica gel adsorbed moisture continuously as the relative humidity increased. However, dried copper sulfate did not adsorb a significant amount of moisture up to 38% relative humidity; a steep increase is observed up to 60% relative humidity, which thereafter slows down and reaches to 33.9% mass gain at 87% relative humidity. The adsorbed amount of moisture increases with the humidity of air and reaches to 30% at 87% relative humidity for silica gel. Copper sulfate-

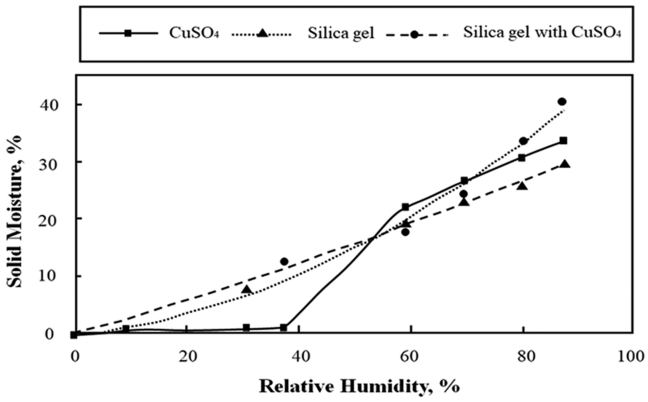

Figure 7. Water vapor adsorption isotherms at 25 °C of silica gel, copper sulfate, and copper sulfate-containing silica gel.

containing silica gel adsorbs lower amount of moisture up to 60% relative humidity and higher amount at higher relative humidity values than those of silica gel. The moisture adsorbed at 87% relative humidity is 30 and 41% for silica gel and copper sulfate-containing silica gel, respectively. The presence of copper sulfate in silica gel affected the moisture adsorption at high relative humidity values, resulting in higher moisture adsorption values than those of the copper sulfate and silica gel.

The adsorption isotherms of water in silica gel and copper sulfate-containing silica gel can be represented by eqs 15 and 16 with R^2 values of 0.99 and 0.97, respectively.

$$q_w = 0.0006\, C_w^2 + 0.286\, C_w \tag{15}$$

$$q_w = 0.0039\, C_w^2 + 0.106\, C_w \tag{16}$$

where q_w is the solid moisture % and C_w is the relative humidity of air at 25 °C.

The presence of copper sulfate in the pores of silica hydrogel during drying resulted in higher pore volume, similar to the silica hydrogel with $(NH_4)_2CO_3$ crystals dried by an antisolvent crystallization involved process.[44] $(NH_4)_2CO_3$ crystals from antisolvent crystallization confined to the pores were significant in preventing the pores from destruction during ambient pressure drying. The total pore volumes of silica gel and silica gel with copper sulfate were found using the Gurvich rule.[45] The volume of the liquid adsorbed closed to the saturation relative humidity is equal to the total pore volume according to the Gurvich rule. Thus, by assuming that water filling the pores has the same density of liquid water, the total pore volumes of silica gel and silica gel with copper sulfate were found as 0.30 and 0.41 $cm^3\ g^{-1}$, respectively. The higher pore volume of silica gel was formed due to the presence of Cu(II) ions in the solution phase. This resulted in the adsorption of higher amount of moisture in Cu(II)-containing silica gel is due to the filling of the additional pore volume.

The pore size distribution of the samples was found by the Kelvin equation. The Kelvin equation gives a relation between the pore size and the capillary condensation pressure[45]

$$RT \ln \frac{P^{con}}{P^{sat}} = -\frac{2\gamma^{\infty} V^{L}}{r_p} \tag{17}$$

where R is the universal gas constant, T is the absolute temperature, P^{con} is the capillary condensation pressure, which is the saturation pressure for the fluid confined in a capillary,

https://dx.doi.org/10.1021/acs.iecr.9b06950
Ind. Eng. Chem. Res. 2020, 59, 9939−9949

P^{sat} is the saturation pressure of the bulk fluid, $\gamma\infty$ is the surface tension between the vapor and liquid phases at the bulk condition, v^L is the molar volume of the liquid phase, and r_p is the pore radius. The r_p values were calculated using the relative pressures (% relative humidity/100) and taking v^L for water as 18 cm^3 mol^{-1} and γ^∞ for water as 72 mN m^{-1}. The total amount adsorbed at each pore size value is shown in Figure 8.

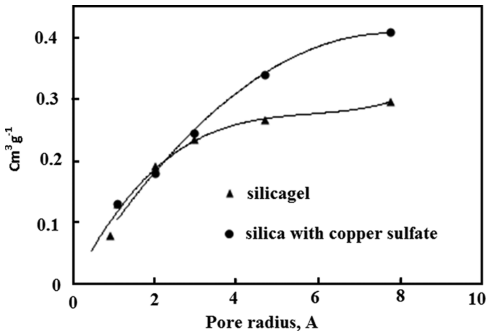

Figure 8. Volume of liquid water adsorbed versus pore radius for silica gel and silica gel with copper sulfate.

IR Analysis. The IR spectra of the dried and moisture-adsorbed samples in Figure 9 give information about the changes caused by moisture adsorption. The main peaks and their vibrations are presented in Table 3.

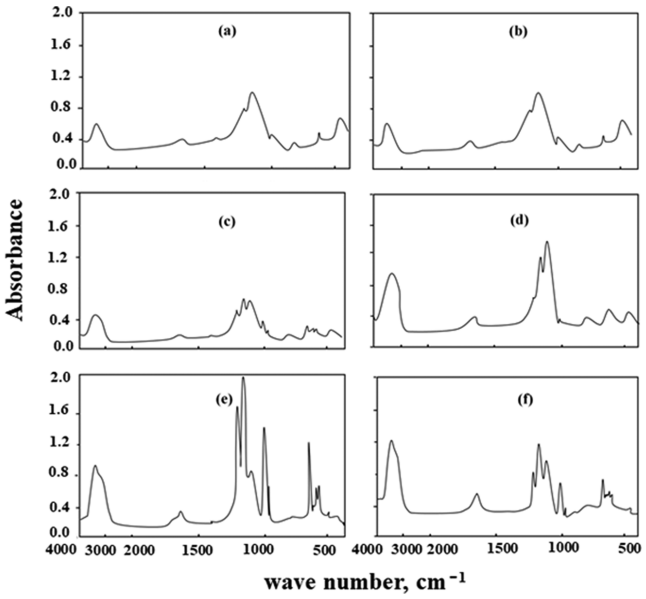

Figure 9. Infrared spectra of (a) dried silica gel, (b) silica gel in equilibrium with 75% relative humidity air at 25 °C, (c) dried silica gel with $CuSO_4$, (d) silica gel with $CuSO_4$ in equilibrium with 75% relative humidity air at 25 °C, (e) dried $CuSO_4$, and (f) $CuSO_4$ in equilibrium with 75% relative humidity air at 25 °C.

The spectra of silica gel in Figure 9a,b had vibrations related to hydrogen-bonded OH groups at 3400 cm^{-1}, free water at 1640 cm^{-1}, Si−O groups at 1160 and 1100 cm^{-1}, and Si−OH groups at 970 cm^{-1}. Symmetric stretching vibrations of Si−O−Si at 800 cm^{-1} and asymmetric stretching vibrations of the Si−O−Si bond at 1100 cm^{-1} were observed in amorphous SiO_2. The weak band at 620 cm^{-1} indicated the presence of a small amount of sulfate ions in silica gel due to the difficulty in the complete removal of sulfate ions by the repeated washing process. The intensities of the hydrogen-bonded OH vibrations and free water vibrations slightly increase by moisture adsorption.

The IR spectra of samples with Cu(II) ions (Figure 9c,d) showed that SO_4^{2-} ions were transferred from the solution phase to the silica hydrogel phase, as concluded from the vibrations of SO_4^{2-} ions present in the spectra. The IR spectrum of silica gel with Cu(II) ions had the vibrations of SiO_2, SO_4^{2-} ions, and H_2O. The spectrum of silica gel having $CuSO_4$ (Figure 8c,d) is the sum of the spectrum of $CuSO_4$ and silica gel, and the bands at 980 and 960 cm^{-1} indicate the presence of Cu−O−Si bands.[45] On adsorption of the moisture, these bands shift to 990 and 980 cm^{-1}. The absorbance of the hydrogen-bonded OH group peak at 3400 cm^{-1} and free water vibration at 1640 cm^{-1} increases with moisture absorption. Also, the symmetry of the vibrations of the sulfate groups changes and their intensity increases.

The vibrations of the hydrated sulfate group in the gas phase were investigated by Zhou et al.[46] The tetrahedrally symmetric sulfate dianion in the gas phase has two infrared-active modes: the antisymmetric stretching ν_3 and bending ν_4 modes at 1106 and 617 cm^{-1}, respectively. The IR spectrum of liquid water also exhibits two bands in this spectral region: the intramolecular bending mode at 1645 cm^{-1} and the intermolecular frustrated rotation, or vibrational mode, at 683 cm^{-1}.[45] The vibrational frequencies of copper sulfate pentahydrate were investigated by Bakr et al.[47] The O−H stretching vibration at 3446 cm^{-1}, the O−H bending vibration at 1629 cm^{-1}, the stretching vibration of the S−O group at 1151 cm^{-1}, the SO_4^{2-} nondegenerate mode at 997 cm^{-1}, the vibration mode of metal ion Cu^{2+} (Cu−O−H) at 785 cm^{-1}, the SO_4^{2-} degenerate mode at 659 cm^{-1}, and the SO_4^{2-} bending group of sulfate at 453 cm^{-1} were observed in the IR spectrum of crystals obtained by the slow evaporation of 0.5 mol dm^{-3} copper sulfate solution.[47]

The vibrations in the $CuSO_4{\cdot}H_2O$ IR spectrum were reported as $\rho(H_2O)$ at 478(m) cm^{-1}; $\nu_4(SO)_4$ at 593(m), 625(m), and 675(m) cm^{-1}; $\rho(H_2O)$ at 805(m) and 870(m) cm^{-1}; $\nu_i(SO)_4$ at 1020(m) cm^{-1}; $\nu_3(SO)_4$ at 1080(s), 1120(s), and 1195(s) cm^{-1}; $\delta(H_2O)$ at 1510(wk) cm^{-1}; and $\nu(H_2O)$ at 3135(s) and 3360(s) cm^{-1}, where w, m, and s indicate weak, medium, and strong, respectively.[40] On the other hand, the vibrations frequencies of $CuSO_4$ are as follows: $\nu_2(SO)_4$ at 496(m) cm^{-1}; $\nu_4(SO)_4$ at 589, 609, and 710 cm^{-1}; $\nu_1(SO)_4$ at 968(s) cm^{-1}; $\nu_3(SO)_4$ at 1083(s), 1095(s), 1155(s), and 1210(s) cm^{-1} (sh), where sh indicates shoulder.[40]

The dried $CuSO_4{\cdot}5H_2O$ was not totally anhydrous $CuSO_4$ since its spectrum in Figure 8e has the hydrogen-bonded OH group vibration at 3400 cm^{-1} and the H_2O bending vibration at 1640 cm^{-1}. On the other hand, the spectrum of $CuSO_4$ shows that the symmetry of the vibrations of the SO_4^{2-} groups does not change but their intensity decreases by moisture absorption, while the intensities of the hydrogen-bonded OH group vibrations and free water vibration intensities increase, as shown in Figure 8f.

X-ray Analysis. The XRD patterns of silica gel and dry copper sulfate-containing silica gel are shown in Figure 10. There are only two broad peaks in the X-ray diffraction pattern of silica gel in Figure 10a. The first peak is at a 2θ value of 10° (0.887 nm) and the second one is at 24°. Silica gel is an amorphous material as concluded from the absences of sharp peaks related to the crystalline material.[48] In the X-ray

https://dx.doi.org/10.1021/acs.iecr.9b06950
Ind. Eng. Chem. Res. 2020, 59, 9939−9949

Table 3. Infrared Peaks of the Dried and Moisture-Adsorbed Samples

	silica gel		silica gel with $CuSO_4$		$CuSO_4$		
vibration	dry	moist	dry	moist	dry	moist	refs
hydrogen-bonded OH stretching ν H_2O	3400(s)	3400(s)	3600(s)	3600(s)	3800(s)	3600(s)	40, 47
H_2O bending	1640(m)	1640(m)	1649(m)	1640	1640(m)	1620(m)	46, 47
	1400(w)	1400(w)	1400(w)	1400(w)		1200(m)	
asymmetric Si−O stretching	1180(sh)	1160(sh)	1200(m)	1160(s)			
	1100(s)	1100(s)	1090(s)	1090(s)			
asymmetric stretching ν_3 $(S-O)_4$ stretching			1090(s)	1090(s)	1140(sh)	1160(s)	46
					1000(s)	960(w)	40
Si−OH stretching	960(w)	970(w)					
surface Cu−O−Si stretching			980(m)	990(w)			46
			960(w)	980(w)			
symmetric Si−O stretching	800(w)	800(w)	800(w)	800(w)			
Cu−O−Si stretching			780(w)	790(m)	770(w)	770(w)	46
ν_4SO_4 bending	620(w)	620(w)		620(m)			40, 47
					600 (s)	600(w)	
					580(s)		
					510(w)		
bending vibration of Si−O−Si	460(m)	460(w)	460(w)	460(m)			

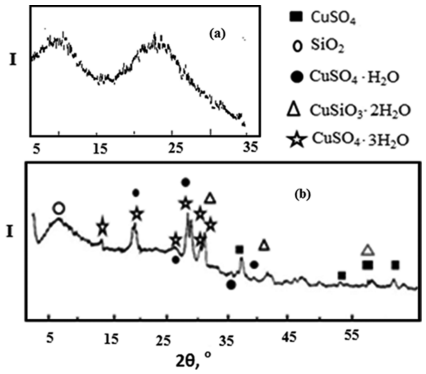

Figure 10. XRD pattern of (a) silica gel and (b) silica gel with copper sulfate.

diffraction pattern of copper-containing silica gel, the broad peak at a 2θ value of 7.18° (1.234 nm) indicated the presence of amorphous silica gel. The first peak in silica gel corresponds to the average interatomic distance in the gel. The average interatomic distance was increased from 0.887[48] to 1.234 nm in silica gel with copper sulfate. In Table 4, the observed and theoretical peaks of probable substances in silica gel with copper sulfate are shown. The peaks at 2θ values of 14.37, 19.83, 23.28, 26.15, 28.45, and 28.89° belonged to $CuSO_4 \cdot 3H_2O$,[49] and the peaks at 2θ values of 19.83, 26,15, 28.45, 35.63, 38.79, and 41.09° and belonged to $CuSO_4 \cdot H_2O$ crystals (JCPDS file number 12-0782).[50]

The peaks at 2θ values of 26.15, 33.05, 37.36, 54.51, 54.47, 58.05, 60.34, and 63.22° could be due to the presence of a small amount of $CuSO_4$.[51]

The formation of copper silicate while preparing silica gel with copper sulfate is also a possibility. Even if silica hydrogel was washed with water ten times for purification to remove unreacted sulfuric acid and byproduct sodium sulfate, a fraction of unreacted sodium silicate would remain in the hydrogel and it would react with copper ions when contacted with the copper sulfate solution. Thus, the fit of the observed diffraction peaks to JCPDS 03-0219 for copper silicate was also checked. A small amount of $CuSiO_3 \cdot 2H_2O$ was present as indicated by the peaks at 19.83, 26.15, 37.36, 57.47, and 63.22° (JCPDS file number 03-0219).[52]

The XRD peaks were broadened due to the small size of the crystals, which was found as 16 nm from the breadth of the diffraction line at a 2θ value of 19.8° using the Scherrer equation (eq 18).

$$L = k\lambda/(B \cos\theta) \tag{18}$$

where L is the crystal size, λ is the wavelength of the X-rays, B is the breadth of the diffraction line (in radians) at diffraction angle θ, and k is a constant that was taken as 0.9 in the present study. The crystals formed in silica hydrogel were nanoparticles. The growth of nanoparticles formed in silica hydrogel stopped due to the confining effect in its pores.[53]

Color. In Figure 11, the colors of silica gel and dried and moisture-adsorbed copper sulfate are shown. While the silica gel (Figure 11a) is colorless, dry copper sulfate $CuSO_4 \cdot H_2O$ (Figure 11) is light blue and moisture-adsorbed copper sulfate ($CuSO_4 \cdot 3H_2O$; Figure 11) is dark blue. Thus, the silica gel with copper sulfate had the same color-changing property upon moisture adsorption.

The visible spectra of silica gel and dry and moist silica gel with $CuSO_4$ are shown in Figure 12. Pristine silica gel had very low absorption of visible light, making it appear as white, and the dry copper sulfate-containing silica gel had increasing absorption intensity of light with the wavelength in 550−700 nm range. The absorbed amount of light is higher for the moisture-adsorbed copper sulfate-containing silica gel than that for its dry form, making it appear dark blue as shown in Figure 12. For this reason, it is thought that the copper sulfate-containing silica gel can be used as a humidity indicator.

It was aimed to produce a humidity-indicating silica gel based on the different colors of copper sulfate hydrates in the present study. The copper sulfate was impregnated to silica hydrogel with 10% SiO_2 and 90% water from aqueous copper sulfate solution and the silica hydrogel phase was dried at 100 °C to obtain indicating silica gel. The silica hydrogel phase was at pH 2 to obtain microporous, granular silica gel.[1] Copper ions were mainly present in the fraction of silica hydrogel pores, which were accessible[28] at this pH value. Since there was no hydrothermal heating in an autoclave at high temperatures,

https://dx.doi.org/10.1021/acs.iecr.9b06950
Ind. Eng. Chem. Res. 2020, 59, 9939−9949

Table 4. Relative Intensities of the Observed Peaks and Theoretical Peaks for Silica Gel with Copper Sulfate

observed, 2θ, nm and intensity			theoretical, nm (intensity)			
2θ (deg)	d (nm)	intensity	$CuSO_4·3H_2O$[49]	$CuSO_4·H_2O$[50] (JCPDS 12-0782)	$CuSO_4$[51]	$CuSiO_3·2HO$[52] (JCPDS 03-0219)
7.18	1.234	48				
14.37	0.618	24	0.509(65)			
19.83	0.449	67	0.44(100)	0.494(30)		0.435(100)
23.28	0.383	10	0.365(54)			
26.15	0.342	14	0.342(50)	0.344(40), 0.347(25), 0339(100)	0.354(100)	0.336(50)
28.45	0.315	100	0.324(67)	0.315(75)		
29.89	0.300	95	0.300(39)			
30.46	0.294	38				0.292(20)
31.03	0.289	71	0.281(43)			0.281(20)
33.05	0.272	14			0.262(95)	
35.63	0.253	10		0.253(18)		
37.36	0.241	48			0.242(50)	0.246(20)
38.79	0.233	10		0.232(25)		
41.09	0.220	24		0.224(16)		
41.67	0.217	19				
43.97	0.207	5		0.21(6)		
45.69	0.199	14				
48.56	0.188	19				
49.43	0.185	14				
54.31	0.169	14			0.171(8)	
57.47	0.161	14			0.163(6)	0.163(10)
58.05	0.159	19			0.160(16)	
60.34	0.154	24			0.157(6)	
63.22	0.148	14			0.143(18)	0.148(80)

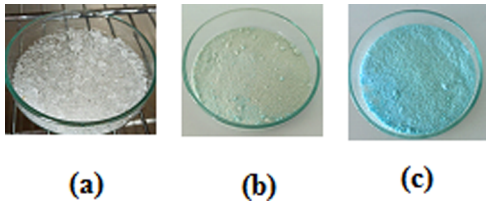

Figure 11. Photographs of (a) silica gel, (b) dry copper sulfate, and (c) moisture-adsorbed copper sulfate.

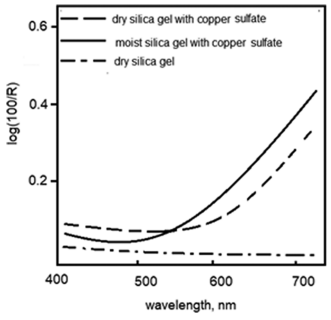

Figure 12. Visible spectra of dry silica gel and dried and moisture-adsorbed silica gel with copper sulfate.

such as 150[20] or 230 °C,[18] the formation of copper silicates was not expected. However, XRD analysis indicated the presence of a small amount of copper silicate hydrate. The DSC analysis indicated that copper-containing silica gel indicated the removal of the crystal water of $CuSO_4·H_2O$ in silica gel occurred at a lower temperature (247 °C), than that (275 °C) of pure $CuSO_4·H_2O$. This could also indicate the possibility of the removal of hydrate water of copper silicate hydrate simultaneously with that of $CuSO_4·H_2O$. The number of smaller pores of silica gel decreased and that of larger pores increased in the case of drying copper sulfate-impregnated silica hydrogel. Thus, copper sulfate-containing silica gel adsorbed higher amount of moisture at high relative humidity values at which larger pores were filled.

The humidity indicator developed in the present study was based on the change of color of copper sulfate crystals with humidity. The humidity-indicating silica gel in dry form contained mainly $CuSO_4·H_2O$, which is light blue. It transformed into dark-blue $CuSO_4·3H_2O$ upon moisture adsorption. However, the samples were partially in the water-adsorbed state in ambient air when their X-ray diffraction patterns were obtained. Thus, $CuSO_4·3H_2O$, $CuSO_4·H_2O$, and surprisingly a small amount of $CuSO_4$ were all detected in the sample by XRD. The small amount of copper silicate present in silica gel was not expected to contribute to the color change.

3. CONCLUSIONS

The equilibrium and kinetics of Cu(II) sorption to silica hydrogel having 15% silica were investigated by contacting 200−1600 mg dm^{-3} Cu(II) ion-containing solutions with silica hydrogel. The adsorption equilibrium best fitted to the Freundlich model, and the adsorption kinetics fitted to the first-order model. The solid diffusion model also has a high R^2 value, and the diffusion coefficient of Cu(II) in silica hydrogel was determined to be 1×10^{-10} m^2 s^{-1}.

The dried gels with copper sulfate were light blue and become dark blue upon moisture adsorption. XRD revealed that the gels contained mainly $CuSO_4·3H_2O$, $CuSO_4·H_2O$, $CuSO_4$, and a small amount of $CuSiO_3·2H_2O$. The prepared copper sulfate-containing gel contained light-blue $CuSO_4·H_2O$, and upon moisture adsorption at 25 °C, it is transformed into dark-blue $CuSO_4·3H_2O$, as clearly shown by visible spectroscopy. Nanoparticles of $CuSO_4·H_2O$ were formed by drying the

https://dx.doi.org/10.1021/acs.iecr.9b06950
Ind. Eng. Chem. Res. 2020, 59, 9939−9949

silica hydrogels impregnated with a saturated copper sulfate solution at 100 °C. The particle size of the crystals in silica gel was about 16 nm. The presence of nanoparticles of copper sulfate in silica gel affected the moisture adsorption at high relative humidity values, resulting in higher moisture adsorption values than those of both copper sulfate and silica gel. The characterization of silica gel containing copper sulfate prepared herein revealed that it can be used as an indicating agent in humidity-adsorbing columns, as aimed.

AUTHOR INFORMATION

Corresponding Author

Devrim Balköse − *Department of Chemical Engineering, Izmir Institute of Technology, Izmir 35430, Turkey;* orcid.org/0000-0002-1117-9486; Phone: +90 533 414 0927; Email: devrimbalkose@gmail.com

Authors

Sevgi Ulutan − *Department of Chemical Engineering, Ege University, Izmir 35100, Turkey*

A. Pinar Tüzüm Demir − *Department of Chemical Engineering, Uşak University, Uşak 64000, Turkey*

Complete contact information is available at: https://pubs.acs.org/10.1021/acs.iecr.9b06950

Author Contributions

All authors contributed equally in writing the manuscript.

Notes

The authors declare no competing financial interest.

ACKNOWLEDGMENTS

This research did not receive any specific grant from funding agencies in the public, commercial, or not-for-profit sectors.

REFERENCES

(1) Balköse, D.; Ulutan, S.; Ozkan, F. C.; Celebi, S.; Ulku, S. Dynamics of water vapor adsorption on humidity-indicating silica gel. *Appl. Surf. Sci.* **1998**, *134*, 39−46.

(2) Rübner, K.; Balkose, D.; Robens, E. Methods of humidity determination Part I: Hygrometry. *J. Therm. Anal. Calorim.* **2008**, *94*, 669−673.

(3) Mukai, S. R.; Nishihara, H.; Tamon, H. Morphology maps of ice-templated silica gels derived from silica hydrogels and hydrosols. *Microporous Mesoporous Mater.* **2008**, *116*, 166−170.

(4) Knight, A. W.; Tigges, A. B.; Ilgen, A. G. Adsorption of copper (II) on mesoporous silica: the effect of nano-scale confinement. *Geochem. Trans.* **2018**, *19*, No. 13.

(5) Ren, Z. Q.; Zhu, X. Y.; Du, J.; Kong, D.; Wang, N.; Wang, Z.; Wang, Q.; Liu, W.; Li, Q.; Zhou, Z. Facile and green preparation of novel adsorption materials by combining sol-gel with ionimprinting technology for selective removal of Cu(II) ions from aqueous solution. *Appl. Surf. Sci.* **2018**, *435*, 574−584.

(6) Xue, X.; Li, F. Removal of Cu(II) from aqueous solution by adsorption onto functionalized SBA-16 mesoporous silica. *Microporous Mesoporous Mater.* **2008**, *116*, 116−122.

(7) Chiron, N.; Guilet, R.; Deydier, E. Adsorption of Cu(II) and Pb(II) onto a grafted silica: isotherms and kinetic models. *Water Res.* **2003**, *37*, 3079−3086.

(8) Gandhi, M. R.; Meenakshi, S. Preparation and characterization of silica gel/chitosan composite for the removal of Cu(II) and Pb(II). *Int. J. Biol. Macromol.* **2012**, *50*, 650−657.

(9) Anderson, H. V.; Hochgesang, F. P. The copper sulfate-sodium silicate reaction. *J. Phys. Chem. A* **1940**, *44*, 439−446.

(10) Balköse, D.; Ozkan, F.; Köktürk, U.; Ulku, S.; Nişli, G.; Ulutan, S. Characterization of hollow chemical garden fibers from metal salts and water glass. *J. Sol−Gel Sci. Technol.* **2002**, *23*, 253−263.

(11) Rauscher, E.; Schuszter, G.; Bohner, B.; Toth, A.; Horvath, D. Osmotic contribution to the flow-driven tube formation of copper-phosphate and copper-silicate chemical gardens. *Phys. Chem. Chem. Phys.* **2018**, *20*, 5766−5770.

(12) Hariu, T.; Arima, H.; Sugiyama, K. The structure of hydrated copper-silicate gels, an analogue compound for natural chrysocolla. *J. Mineral. Petrol. Sci.* **2013**, *108*, 111−115.

(13) Jin, R. X.; Yang, Y.; Zhang, Y.; Li, W.; Gan, W.; Xuet, J. Facile Synthesis and Properties of Hierarchical Double-Walled Copper Silicate Hollow Nanofibers Assembled by Nanotubes. *ACS Nano* **2014**, *8*, 3664−3670.

(14) Wang, Y.; Wang, G. Z.; Wang, H.; Cai, W.; Zhang, L. One-pot synthesis of nanotube-based hierarchical copper silicate hollow spheres. *Chem. Commun.* **2008**, *48*, 6555−6557.

(15) Zhan, G. W.; Zeng, H. C. Topological Transformations of Core-Shell Precursors to Hierarchically Hollow Assemblages of Copper Silicate Nanotubes. *ACS Appl. Mater. Interfaces* **2017**, *9*, 37210−37218.

(16) Lopes, A. M. L.; Lin, Z.; Ferdov, S. Rapid and phase pure synthesis of microporous copper silicate (CuSH-1Na) with 12-ring channel system. *J. Porous Mater.* **2018**, *25*, 1309−1316.

(17) Wang, X.; Liu, L. M.; Jacobson, A. J. Nanoporous copper silicates with one-dimensional 12-ring channel systems. *Angew. Chem., Int. Ed.* **2003**, *42*, 2044−2047.

(18) Datta, S. J.; Khumnoon, C.; Lee, Z. H.; 1 Moon, W. K.; Docao, S.; Nguyen, T. H.; Hwang, I. C.; Moon, D.; Oleynikov, P.; Terasaki, O.; Yoon, K. B. CO2 capture from humid flue gases and humid atmosphere using a microporous coppersilicate. *Science* **2015**, *350*, 302−306.

(19) Tobin, Z. M.; Posada, L. F.; Bechu, A. M.; Carroll, M. K.; Bouck, R. M.; Anderson, A. M.; Bruno, B. A. Preparation and characterization of copper-containing alumina and silica aerogels for catalytic applications. *J. Sol−Gel Sci. Technol.* **2017**, *84*, 432−445.

(20) Jiang, J. W.; Tu, C. C.; Chen, C.-H.; Yu Lin, Y.-C. Highly Selective Silica-supported Copper Catalysts Derived from Copper Phyllosilicates in the Hydrogenation of Adipic Acid to 1,6-hexanediol. *ChemCatChem* **2018**, *10*, 5449−5458.

(21) Zhang, M.; Wang, B. Y.; Yanwei Zhang, Y.; Weizhen Li, W.; Gan, W.; Xu, J. Facile synthesis of magnetic hierarchical copper silicate hollow nanotubes for efficient adsorption and removal of hemoglobin. *Dalton Trans.* **2016**, *45*, 922−927.

(22) Zhang, M.; Wang, Y. T.; Yanwei Zhang, Y.; Lei Ding, L.; Jing Zheng, J.; Jingli Xu, J. Preparation of magnetic carbon nanotubes with hierarchical copper silicate nanostructure for efficient adsorption and removal of hemoglobin. *Appl. Surf. Sci.* **2016**, *375*, 154−161.

(23) Baltacioğlu, H.; Balkose, D. Diffusion of Protons in Silica Hydrogel. *Colloid Polym. Sci.* **1989**, *267*, 460−464.

(24) Ulutan, S. Kinetics of Adsorption and Diffusion of Cu(II) in Silica Hydrogel. In *Third National Chemical Engineering Congress Proceedings*,Saraç, H.; Çopur, M.; Kurtbaş, A.; Levent, M.; Laçin, O.; Temur, H.; Demir, F.; Beşe, V., Eds.; Atatürk University: Erzurum, Turkey, 1998; pp 364−367.

(25) Balköse, D.; Baltacıoğlu, H.; Ulutan, S.; Köktürk, U. Characterization of Silica Gel Modified with Copper Sulfate. In *Third National Chemical Engineering Congress Proceedings*,Saraç, H.; Çopur, M.; Kurtbaş, A.; Levent, M.; Laçin, O.; Temur, H.; Demir, F.; Beşe, V., Eds.; Atatürk University: Erzurum, Turkey, 1998; pp 1180−1185.

(26) James, R. O.; Healy, T. W. Adsorption of hydrolyzable metal-ions at oxide water interface. 1. Co(II) adsorption on SiO2 and TiO2 as model syatems. *J. Colloid Interface Sci.* **1972**, *40*, 65.

(27) Iler, R. K. *Chemistry of Silica*; Wiley: NewYork, 1979; p 180.

(28) Blomqvist, C. H.; Geback, T.; A. Altskär, A.; Hermansson, A.-M.; Gustafsson, S.; Lorén, N.; Olsson, E. Interconnectivity imaged in three dimensions: Nano-particulate silica-hydrogel structure revealed using electron tomography. *Micron* **2017**, *100*, 91−105.

(29) Ulutan, S.; Atakul, S.; Balkose, D. Washing of Silica Hydrogel, Equilibrium, and Kinetics of Co(II) Sorption for Production of Humidity Indicating or Catalyst Silica Gel. In *Chemistry And Industrial Techniques For Chemical Engineers*,Pogliani, L.; Ameta, S. C.; Haghi, A. K., Eds.; Apple Academic Press: Toranto, 2020; pp 123−145.
(30) Kaczmarek, M.; Kazimierska-Drobny, K. Estimation-identification problem for diffusive transport in porous materials based on single reservoir test: Results for silica hydrogel. *J. Colloid Interface Sci.* **2007**, *311*, 262−275.
(31) Kaczmarek, M.; Kazimierska-Drobny, K. Identification problem of interface boundary conditions for diffusive transport between water and silica hydrogel. *Mater. Sci.-Pol.* **2007b**, *25*, 851−859.
(32) Ribeiro, A. C. F.; Lobo, V. M. M.; Natividade, J. J. S. Diffusion Coefficients in Aqueous Solutions of Cobalt Chloride at 298.15 K. *J. Chem. Eng. Data* **2002**, *47*, 539−541.
(33) Ribeiro, A. C. F.; Esteso, M. A.; Lobo, V. M. M.; Valente, A. J. M.; Simoes, S. M. N.; Sobral, A. J. F. N.; Burrows, H. D. Diffusion coefficients of copper chloride in aqueous solutions at 298.15 K and 310.15 K. *J. Chem. Eng. Data* **2005**, *50*, 1986−1990.
(34) Keserova, G. M.; Shamrikov, V. M.; Malkimon, V. I.; Belotserskovskoya, N. G. *USSR Applied Chemistry* **1987**, *4*, 882−885.
(35) Pathak, P. N.; Choppin, G. R. Effects of pH, Ionic Strength, Temperature, and Complexing Anions on the Sorption Behavior of Cobalt on Hydrous Silica. *Soil Sediment Contam.* **2009**, *18*, 590−602.
(36) Tantemsapya, N.; Meegoda, J. N. Estimation of diffusion coefficient of chromium in colloidal silica using digital photography. *Environ. Sci. Technol.* **2004**, *38*, 3950−3967.
(37) Perullini, M.; Jobbagy, M.; Japas, M. L.; Nilmes, S. S. New method for the simultaneous determination of diffusion and adsorption of dyes in silica hydrogels. *J. Colloid Interface Sci.* **2014**, *425*, 91−95.
(38) Ruggiero, M. T.; Erba, A.; Orlando, R.; Korter, T. M. Origins of contrasting copper coordination geometries in crystalline copper sulfate pentahydrate. *Phys. Chem. Chem. Phys.* **2015**, *17*, 31023−31029.
(39) Moore, W. J. *Physical Chemistry*; Longmans&Green: London, 1963; p 144.
(40) Haber, V. Study of the amorphous product of dehydration of copper (II) sulfate pentahydrate. *Chem. Zvesti* **1977**, *31*, 190−196.
(41) de Castelnuovo, S.; Harness, J. B.; McColm, I. J. The role of liquid water in crystalline hydrate dehydration. Copper sulphate pentahydrate. *J. Therm. Anal. Calorim.* **2001**, *63*, 233−247.
(42) Cheng, L.; Li, W.; Li, Y.; Yang, Y.; Li, Y.; Cheng, Y.; Song, D. Thermal analysis and decomposition kinetics of the dehydration of copper sulfate pentahydrate. *J. Therm. Anal. Calorim.* **2019**, *135*, 2697−2703.
(43) White, R. L. Variable temperature infrared study of copper sulfate pentahydrate dehydration. *Thermochim. Acta* **2012**, *528*, 58−62.
(44) Asare Bediako, B. B.; Cao, J. Y.; Liu, Q.; Li, J. An antisolvent crystallization involved process for drying silica hydrogel. *Drying Technol.* **2019**, *37*, 1605−1614.
(45) Ongari, D.; Boyd, P. G.; Barthel, S.; Witman, M.; Haranczyk, M. Accurate Characterization of the Pore Volume in Microporous Crystalline Materials. *Langmuir* **2017**, *33*, 14529−14538.
(46) Zhou, J.; Santambrogio, G.; Brümmer, M.; Moore, D. T.; Wöste, L.; Meijer, G.; Neumark, D. M.; Asmis, K. R. Infrared spectroscopy of hydrated sulfate dianions. *J. Chem. Phys.* **2006**, *125*, No. 111102.
(47) Bakr, N. A.; Al-Dhahir, T. A.; Mohammad, S. B. Growth of Copper Sulfate Pentahydrate Single Crystals by Slow Evaporation Technique. *J. Adv. Phys.* **2017**, *13*, 4651−4656.
(48) Balköse, D.; Kokturk, U.; Yılmaz, H. A study of cobaltous chloride dispersion on the surface of the silica gel. *Appl. Surf. Sci.* **1999**, *147*, 77−84.
(49) Zahrobsky, R. F.; Bauer, W. H. On the crystal chemistry of salt hydrates. V. The determination of the crystal structure of CuSO4.3H2O (bonattite). *Acta Crystallogr., Sect. B: Struct. Crystallogr. Cryst. Chem.* **1968**, *24*, 508−513.
(50) Joint Committee on Powder Diffraction Standards (JCPDS file number 12-0782)
(51) Gaines, R. V.; Skinner, H. C. W.; Foord, E. E.; Mason, B.; Rosenzweig, A. *Dana's New Mineralogy*, 8th ed.; Wiley-Interscience; New York, 1997.
(52) Joint Committee on Powder Diffraction Standards (JCPDS file number 03-0219)
(53) Seok, S. I.; Kim, J. H. TiO2 nanoparticles formed in silica sol-gel matrix. *Mater. Chem. Phys.* **2004**, *86*, 176−179.

https://dx.doi.org/10.1021/acs.iecr.9b06950
Ind. Eng. Chem. Res. 2020, 59, 9939−9949